ARTICLE OPEN

Check for updates

Steel rust layers immersed in the South China Sea with a highly corrosive *Desulfovibrio* strain

Xucheng Dong[1,2,3,4], Xiaofan Zhai[1,2,4,5,6]✉, Yimeng Zhang[1,2,4], Jing Yang[1,2,4], Fang Guan[1,2,4], Jizhou Duan[1,2,4,5,6]✉, Jiawen Sun[1,2,3,4], Ruiyong Zhang[1,2,4] and Baorong Hou[1,2,4,5,6]

Although it is well known that microbes play a significant role in marine corrosion, few studies have systematically studied the relationship between microorganisms and corrosion products under long-term immersion. In this study, the corrosion characteristics of the rust layer formed on carbon steel immersed in the South China Sea for 5.5 years were investigated using various surface analysis and microbial community analysis techniques. Magnetite (Fe_3O_4), iron sulfide, and green rust were identified in the inner rust layer. The middle rust layer was composed of maghemite (γ-Fe_2O_3), and some Fe_3O_4 and mackinamite were also detected. The outer rust layer contained several Fe(III)-oxyhydroxides, and it had a large number of fouling organisms attached to it. In all of the rust layers, anaerobic sulfate-reducing bacteria (SRB) were the dominant bacteria, and they may have played a key role in the formation of the corrosion products. One SRB strain (*Desulfovibrio bizertensis* SY-1) with a highly corrosivity (13.561 mg/cm^2) was isolated from these rust layers, and its physiological and metabolic characteristics were studied. These results expand the membership of corrosive SRB and establish a better understanding of marine microbiologically influenced corrosion (MIC).

npj Materials Degradation (2022)6:91 ; https://doi.org/10.1038/s41529-022-00304-7

INTRODUCTION

Owing to the excellent working performance and process characteristics, steel structures are widely used in marine engineering and construction[1]. However, steel structures immersed in seawater usually suffer severe marine corrosion, which is a serious and worldwide problem that has a negative economic impact[2]. Thus, many researchers have focused on the formation of corrosion products in marine environments[3–7]. Carbon steel corrosion products may be separated into two layers: an orange exterior rust layer composed of iron oxyhydroxide, and a black interior rust layer composed of iron sulfide[8]. Moreover, green sulfate rust (GR(SO_4^{2-})) is more likely to form in the inner rust layer's anodic zones, whereas magnetite (Fe_3O_4) forms in the cathodic zones[4]. Corrosion products can remain stable over a long period of time[9].

In marine environments, ubiquitous microbes can participate in the corrosion process and have a substantial impact on metal corrosion products[10–12]. This process is often referred as microbiologically influenced corrosion (MIC) or biocorrosion[13–15]. Molecular biological methods have been used to study the microbial communities in steel rust layers[16,17]. The most frequently reported microbial population in carbon steel rust layers is sulfate-reducing bacteria (SRB) according to the study of microbial community compositions[18]. Smith et al.[10] analyzed the corrosion products of a steel pile and conducted metagenomic analysis of the bacterial communities in accelerated low water corrosion (ALWC) and found that the microorganisms in the rust layer played a key role in the sulfur redox cycle.

Based on these studies, bacteria are commonly considered to dramatically affect the formation of corrosion products[19–21]. Robert et al.[22] described the conversion process from Fe(0) to iron oxide and iron-sulfur compounds under the influence of bacteria. Refait et al.[4] also found that anaerobic bacteria played an important role in the formation of green rust. Furthermore, Sun et al.[23] observed that iron-oxidizing bacteria (IOB) were involved in the synthesis of α-FeOOH, while iron-reducing bacteria (IRB) and anaerobic environments contributed to the formation of Fe_3O_4. In addition, microorganisms can also induce severe localized corrosion, which leads to dangerous perforation of steel sheet piles[24].

Although it is well known that microbes play a significant role in the corrosion of steel in marine environments, few studies have systematically studied the composition of the corrosion products, and the relationship between microorganisms and corrosion products under long-term immersion.

To our knowledge, such accelerated corrosion phenomena in marine environments are generally associated with SRB[25–27]. It was estimated that for all MIC, corrosion loss induced by SRB accounted for more than 50%[28]. Bacteria and archaea, which possess sulfate reducing abilities, can use sulfate as a terminal electron acceptor in their energy metabolism[29,30]. Moreover, the metabolic process of SRB contributes significantly to the global sulfur cycle[31]. Recent research has shown that electroactive SRB may utilize Fe(0) as a single electron source for sulfate reduction[32,33].

Therefore, studying the corrosion process of SRB isolated from marine environments is necessary[34–36]. Dinh et al.[33] reported a novel marine corrosive *Desulfovibrio ferrophilus* strain IS5 with a corrosion rate of 0.2 mg/cm^2 for carbon steel after 7 days of exposure. Duan et al.[35] also isolated and cultivated the electrically

[1]Key Laboratory of Marine Environmental Corrosion and Bio-fouling, Institute of Oceanology, Chinese Academy of Sciences, 7 Nanhai Road, Qingdao 266071, China. [2]Open Studio for Marine Corrosion and Protection, Pilot National Laboratory for Marine Science and Technology (Qingdao), 168 Wenhai Middle Road, Qingdao 266237, China. [3]University of Chinese Academy of Sciences, 19 (Jia) Yuquan Road, Beijing 100039, China. [4]Center for Ocean Mega-Science, Chinese Academy of Sciences, 7 Nanhai Road, Qingdao 266071, China. [5]Sanya Institute of Ocean Eco-Environmental Engineering, Zhenzhou Road, Sanya 572000, China. [6]Institute of Marine Corrosion Protection, Guangxi Academy of Sciences, Nanning 530007, China. ✉email: zhaixf@qdio.ac.cn; duanjz@qdio.ac.cn

active *Desulfovibrio caledoniensis* from a carbon steel rust layer after 1 year of exposure to seawater and proposed the anaerobic corrosion mechanism of steel. Moreover, many researchers have also successfully isolated and cultured SRB from several specific water environments. For example, Musat et al.[37] enriched two strains (NaphS3, NaphS6) from a Mediterranean sediment with the addition of naphthalene. Kniemeyer et al.[38] enriched strain BuS5, which is capable of biodegrading short-chain hydrocarbons using propane or n-butane as the only growing substrate. Microorganisms in corroded steel pile samples at the ALWC were also enriched by Beech et al.[39], and they found that sulfur-oxidizing bacteria (SOB) and SRB coexisted. However, the corrosion behaviors of different SRB are quite different, so it is still of great significance to separate and cultivate potentially highly corrosive SRB from marine environments.

Thus, in this study, Q345 carbon steel was immersed in the South China Sea for 5.5 years to study the interactions between the microorganisms and rust layers. After 5.5 years, the coupons and the environmental seawater samples were retrieved. The composition/structure and formation mechanism of the rust layers were characterized, and the microbial communities were also studied using 16S ribosomal ribonucleic acid (rRNA). A highly corrosive SRB strain was isolated from these rust layers, and the physiological and metabolic characteristics of this strain were studied. It is of great significance to expand the membership of corrosive SRB and to gain a deeper understanding of marine MIC.

RESULTS AND DISCUSSION

Characterization of the rust layers on Q345 steel after immersion in the South China Sea for 5.5 years

The cross-section of the Q345 coupons (Fig. 1) revealed three distinct layers based on color: a dark-green innermost layer (referred to as IL, ~1 mm thick), a black second/middle layer (referred to as ML, ~8–10 mm thick), and a grey and red outermost layer (referred to as OL, ~2–3 mm thick). The rust layers generated on carbon steel were analyzed to obtain a better understanding of the corrosion mechanisms using scanning electron microscopy (SEM) (Fig. 2), X-ray diffraction (XRD) (Fig. 3a), μ-Raman spectroscopy (Fig. 3b), Fourier transform infrared spectroscopy (FT-IR) (Fig. 3c), and X-ray photoelectron spectroscopy (XPS) (Figs. 3d and 4).

In the IL, a large number of spherical and lamellar corrosion products, as well as some irregular block-shaped corrosion products were observed. It should be noted that rod-liked bacteria were also detected (Fig. 2a). As is shown in Fig. 3a, the crystalline diffraction peaks of magnetite (Fe_3O_4), green rust, and iron sulfide were identified in the XRD spectra of the IL. Typical Raman spectra of the IL are shown in Fig. 3b. In the dark-green regions of this layer, magnetite with characteristic Raman peaks at 550 and 670 cm^{-1} was detected[40,41]. The weak peak at 207 cm^{-1} may indicate the presence of nanocrystalline mackinawite[42,43]. The peaks at 430 and 489 cm^{-1} may correspond to the green rust[44],

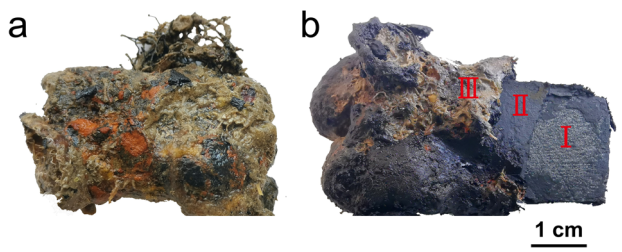

Fig. 1 Optical images of Q345 coupons after 5.5 years-immersion in Sanya nature sea water. a The overall appearance and **b** the profile showing cross sections. (I) dark-green innermost layer (IL), (II) black middle layer (ML), (III) grey and red outermost layer (OL).

but previous studies have also reported that there is a competitive relationship between the formation of magnetite and green rust[45].

Figure 3c shows FT-IR analysis results. The strongest absorbance at 1140 cm^{-1} was attributed to sulfide. The absorbance at 796 cm^{-1} was attributed to Fe–OH stretching. The peaks at 1652 and 1422 cm^{-1} corresponded to the asymmetric and symmetric stretching of carboxylate in the side chain, respectively. In addition, the O–H stretching vibrations of the hydroxyl groups appeared as a large band at 3324 cm^{-1} [10,46].

Figures 3d and 4 show the high resolution XPS spectra of the three rust layers. Basically, the spectrum of C1*s* contained three peaks (Fig. 4a): a C–C peak at 284.72 eV, a C-N peak at 286.37 eV, and a C=O peak at 288.5 eV. The spectrum of O1*s* was curve-fitted with six peaks (Fig. 4b). The peaks at 529.7 and 531.0 eV corresponded to Fe(II)–O and Fe(III)–O, respectively. The peaks at 530.75, 531.44, 533.14, and 533.18 eV were attributed to H–O, SO_4^{2-}, C=O, and NO_3^-, respectively. It was found that the Fe2$p_{3/2}$ iron spectrum consisted of the following four peaks: an iron peak (Fe^0) at 707.94 eV, a divalent oxide peak (Fe^{2+}) at 709.95 eV, a trivalent oxide peak (Fe^{3+}) at 711.07 eV, and an iron sulfide peak at 712.74 eV in IL (Fig. 4c). Regarding the S2$p_{3/2}$ binding energy (Fig. 4d), the sulfur speciation was almost completely dominated by SO_4^{2-} at 168.58 eV and HS^- at 163.7 eV. There was only a small component of FeS at 161.52 eV[10,47–49]. The XRD and Raman results corroborate the XPS findings for all of the main phases of the components.

These results illustrate that the main corrosion products in the IL were magnetite, and a small amount of green rust and iron sulfide was also detected.

In the ML, acicular-like and some flake-like structures were observed, and a few sphere-like products were also detected (Fig. 2c, d). More corrosion product phases were identified in the ML than in the IL. It was found that a large amount of maghemite (γ-Fe_2O_3) was present according to the XRD patterns[50]. The diffraction peaks of magnetite and mackinawite were also observed, which were similar to the composition of the IL.

Raman spectra peaks (Fig. 3b) for a black area of corrosion in the ML were clearly visible at 266, 307, 400, 487, and 717 cm^{-1}. The peaks at 717 and 487 cm^{-1} were assigned to maghemite[51–53], which was determined to be the dominant component of this layer. The strong peak at 266 cm^{-1} could belong to mackinawite[54]. The two weak peaks at 307 and 400 cm^{-1}, which may have corresponded to magnetite and akaganeite (β-FeOOH), respectively. Akaganeite, a type of marine atmospheric corrosion product, may have formed during the post-processing (i.e., during the separation and/or drying processes) in the laboratory, which was difficult to avoid[45].

The FT-IR results (Fig. 3c) for the ML were similar to those for the IL. However, the absorption peak at 1140 cm^{-1} was weak, indicating that this layer had a lower sulfide content. Regarding the XPS fitting results (Fig. 4e–h), no peaks of Fe^0 were found in the ML but peaks for iron oxyhydroxide at 712.31 eV (Fe2$p_{3/2}$) and 531.07 eV (S2$p_{3/2}$) were detected.

As a result, the main corrosion product formed in the ML were determined to be maghemite, but other components such as mackinawite and magnetite were detected as well. Owing to the continual structural modification during the long-term seawater immersion, relatively stable corrosion products likely formed in the ML rather than the IL. Yang et al.[55] also reported similar structures in marine environments, supporting these results.

Non-crystalline structures and fouling organisms were observed in the OL (Fig. 2e). For instance, the smooth, roughly oval-shaped objects were identified as diatoms (Fig. 2f).

Numerous phases were identified via XRD analysis (Fig. 3a). The main corrosion products in the OL were Fe(III)-oxyhydroxides, including goethite (α-FeOOH), lepidocrocite (γ-FeOOH), and a small amount of maghemite. Highly crystalized quartz (SiO_2),

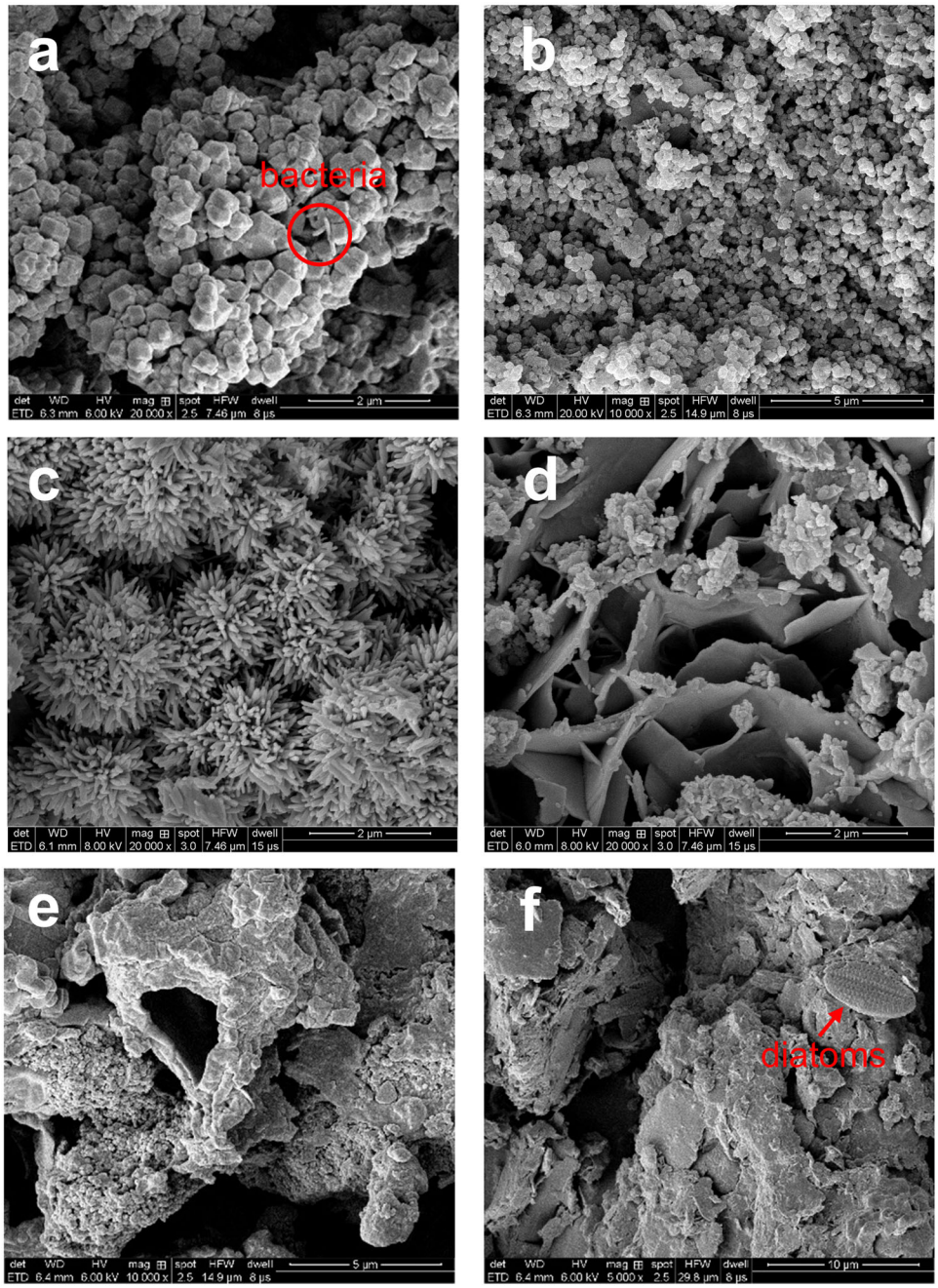

Fig. 2 SEM images of the rust layers of Q345 steel immersed in nature sea water. a, **b** Inner layer, **c**, **d** middle layer, and **e**, **f** outer layer.

halite, and clays from shattered shells were also detected in this layer.

The Raman spectrum (Fig. 3b) exhibited a strong peak at 240 cm^{-1}, which was identified as the characteristic peak of γ-FeOOH[56,57]. The strong peak at 490 cm^{-1} and the comparatively weak peak at 301 cm^{-1} were related to α-FeOOH[58]. Similar to the ML, the peak at 400 cm^{-1} was attributed to β-FeOOH. In addition, a ghost peak at 171 cm^{-1} appeared due to the 532 nm laser[3].

The FT-IR results for the OL showed the strongest absorbance at 1485 cm^{-1} from C–C stretching, which resulted from the attachment of small fouling organisms. The strong band corresponded to C–H stretching vibrations was also detected at 864 cm^{-1}, which indicated the presence of certain organic compounds in this layer. The XPS results for the Fe2*p* and S2*p* in the OL (Fig. 4i–l) were consistent with those for the ML. Owing to the low N content (as shown in Supplementary Table 1), the OL did not exhibit a C–N peak, but it did exhibit a C–Cl peak at 288.71 eV. For O1*s*, the unique SiO_2 spectrum was also detected at 532.88 eV.

Thus, Fe(III)-oxyhydroxides were the main corrosion products, along with a small amount of magnetite. In addition, large amounts of fouling organisms were also found owing to the direct contact between the OL and the sea water.

According to Fig. 3d and Table 1, from the IL to the OL, the nitrogen content decreased and the chlorine content increased. In the OL, silicon (Si) was found, and the iron content was relatively low, which may have been caused by the existence of fouling organisms such as coral and diatoms. Among these three layers, the IL had the lowest oxygen content, which was the result of the

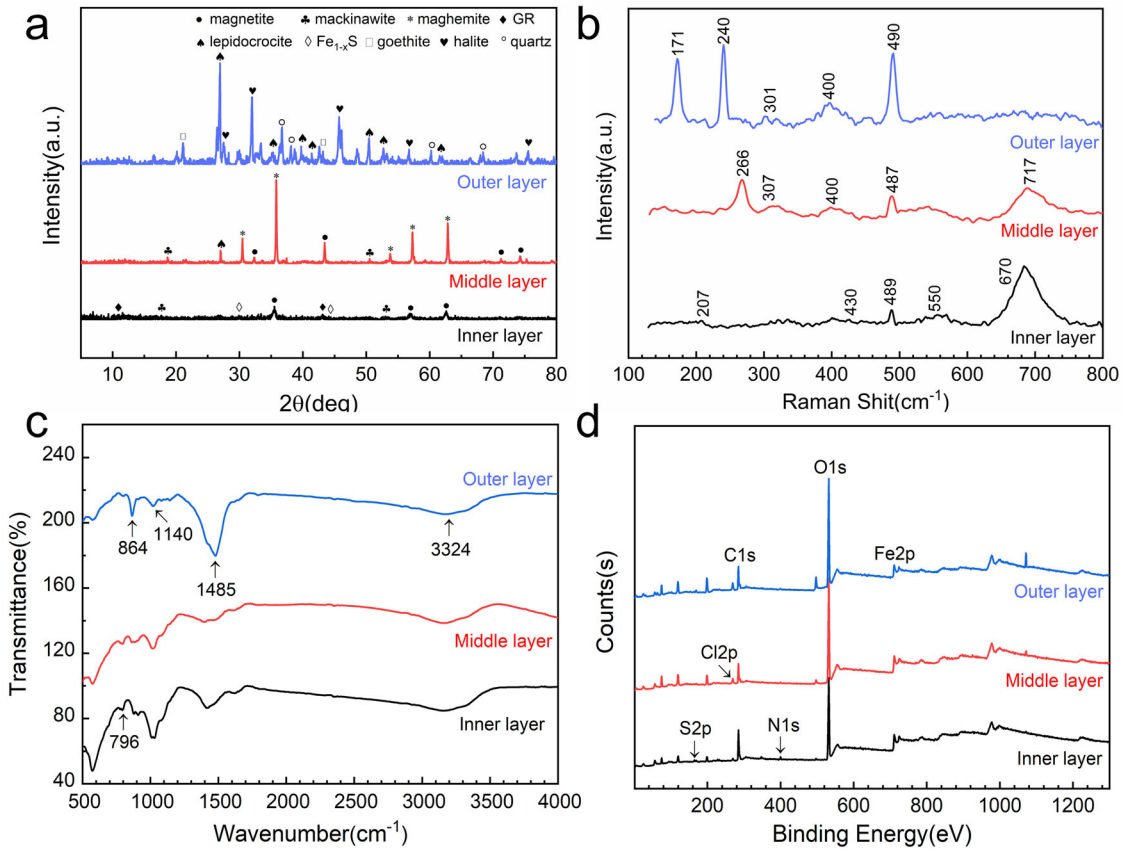

Fig. 3 Composition of the three-rust-layer corrosion products of Q345 steel immersed in nature sea water. a XRD, **b** Raman, **c** FT-IR, and **d** wide-scan XPS spectra.

diffusion and consumption of dissolved oxygen by aerobic microorganisms.

The fitting results of the XPS narrow scan spectra are presented in Fig. 4 and Table 2. It was found that the ratio of the divalent iron oxide Fe(II) decreased from the IL to the OL, while the Fe(III) increased. The low oxygen content led to a low iron oxidation degree in the IL. In addition, the IL had the lowest sulfate content and the highest sulfide content. The sulfate and sulfide contents of the ML and OL were similar. Moreover, iron sulfide was only present in the IL, probably due to the activity of SRB, which has been reported in previous studies[45].

Microbial community analysis of three rust layers

The microorganisms were studied at the class level and genus level to identify the representative taxa that responded positively to metal corrosion. The common and unique operational taxonomic units (OUTs) in the three rust layers were displayed and analyzed using a Venn diagram (Supplementary Fig. 4). The IL, ML, and OL contained 199 (13% of total OTUs), 106 (7% of total OTUs), and 366 (25% of total OTUs) unique OTUs, respectively. According to the rarefaction curves (Supplementary Fig. 3), the 16S rRNA gene sequences obtained in this study, which were generated from the corrosion samples, represented the entire bacterial population.

Figure 5a shows that the prokaryotic phyla comprised 91.57% of the overall community in the rust layer samples, and more than 11 phyla were detected in these samples. *Proteobacteria* was the most common phylum in the ML and OL, accounting for 19.49 to 52.67% of all of the phyla; however, *Chloroflexi* was the most common phylum in the IL (33.60%).

More than 65 genera were identified (Supplementary Fig. 1). *Desulfovibrio* and *Desulfobacter* were the most common bacterial genera in the top 100 according to the hierarchical clustering heat map (Supplementary Fig. 2). *Desulfovibrio* was the most abundant genera, accounting for 1.63, 37.43, and 6.43% of the total number of genera in the IL, ML, and OL, respectively (Fig. 5b and Table 3); and *Desulfobacter* was the second most abundant phylum, accounting for 0.55, 6.69, and 0.64% in the IL, ML, and OL, respectively. The average abundance study revealed that several other genera were well-represented (e.g., *Gammaproteobacteria* and *Ralstonia*). In all of the rust layers, the anaerobic SRB became the dominant bacteria, and the abundances of the SRB in the different rust layers were quite different.

The distinct rust layers had microbial populations with different compositions based on the unweighted pair group method with arithmetic mean (UPGMA) (Supplementary Fig. 6). Alpha diversity analysis was conducted to determine the quantity and diversity of the microbial population in each rust layer, and Table 3 presents the significantly different microbial populations of the different rust layers. The microbial communities in the seawater samples were more diverse and complex than those in the rust layers. The diversity of the microorganisms was the lowest in the ML. The community abundance and diversity of the IL and OL were similar. A similar trend was also observed on the non-metric multi-dimensional scaling (NMDS) plots of the Bray-Curtis distances (Supplementary Fig. 5), which were based on the OTUs.

The functionalities of the microbial communities in all of the rust layers were also analyzed. The high *dsrA* and *dsrB* (0.32%) genes in the ML revealed that dissimilatory sulfate and sulfite reduction and oxidation reactions were the main reactions and were much higher than those in the IL (0.0097%) and OL (0.0057%). The sulfate reductase gene (*dsrAB*) is an important gene

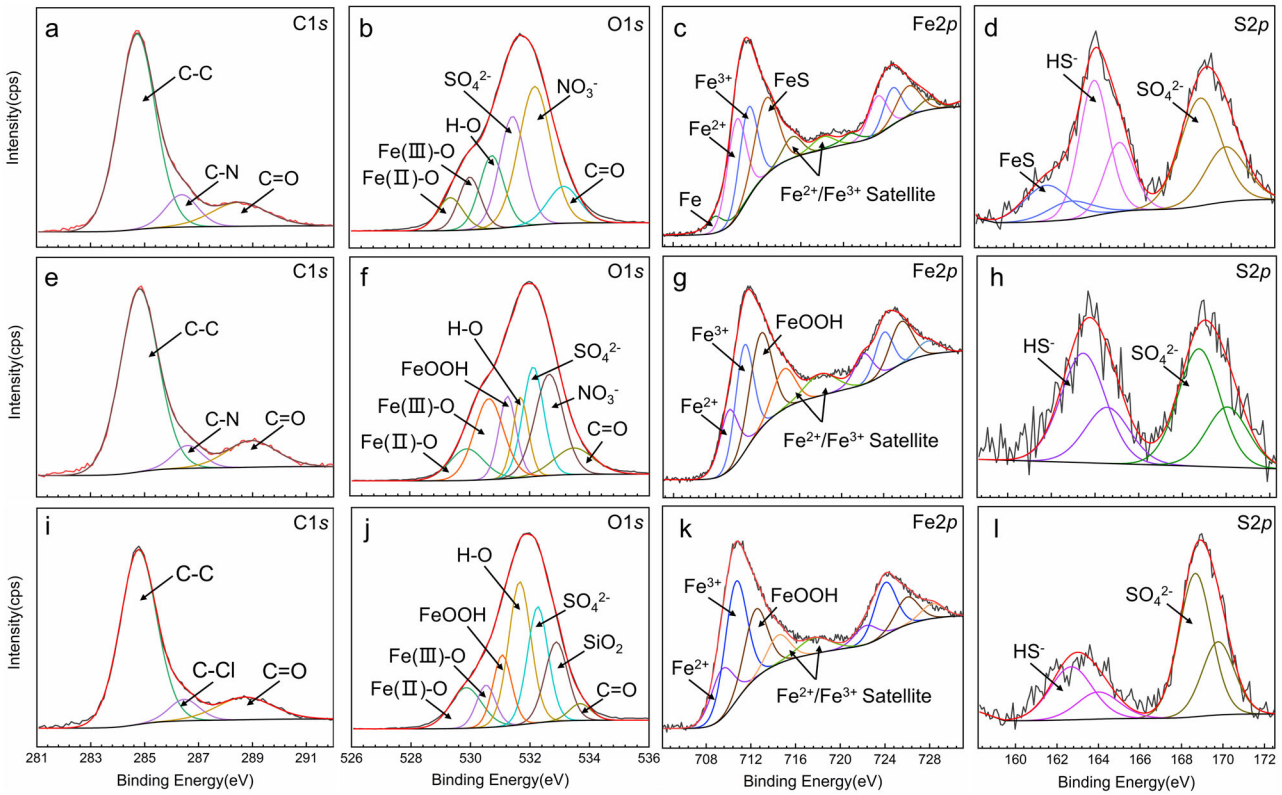

Fig. 4 XPS narrow scan spectroscopy of the corrosion products. a–d Inner layer, **e–h** middle layer, and **i–l** outer layer.

Table 1. Substance content in three rust layers obtained by wide-scan XPS fitting (at%).

	C1s	O1s	Fe2p	S2p	N1s	Cl2p	Si2p
IL	38.86	47.11	6.11	2.40	2.83	2.70	–
ML	26.83	58.75	6.65	1.67	1.02	5.09	–
OL	29.58	55.08	4.52	2.26	–	7.47	1.10

Table 2. Substance content in each valence state by narrow-scan XPS fitting (%).

	Fe(II)/ Fe(Total) (%)	Fe(III)/ Fe(Total) (%)	SO_4^{2-}/ S(Total) (%)	HS^-/ S(Total) (%)
IL	57.33	32.88	44.06	39.97
ML	25.26	74.74	97.71	2.29
OL	21.09	78.91	96.90	3.10

in the anaerobic sulfate metabolism process of SRB, and it has been used as a biomarker to detect and monitor the diversity and abundance of SRB in target samples. In the three rust layers, the *Sat* genes were detected, which could be related to assimilatory sulfate reduction.

SRB and other microorganisms were crucial to forming the corrosion products in the rust layers. The preponderance of iron sulfide in the IL layer revealed a high level of SRB activity. Castaneda et al.[59] reported that the metabolic activity of SRB results in the generation of FeS. The formation process of the green rust may also have been related to the aerobic bacteria in the IL. Duan et al.[35] also reported similar findings. The contents of the divalent and trivalent iron oxides in the ML and OL were similar. Due to the presence of typical IOB (*Pseudomonadales*) and IRB (*Shewanellaceae*) in these two rust layers (Supplementary Fig. 2), the conversion between the different iron oxides was balanced. However, the abundance of this type of microorganism in the rust layer community was very low. In addition, the corrosion products also exerted great influence on the abundance and diversity of the bacteria. For the ML, due to the large amount of FeOOH, which acted as the electron acceptor for the SRB[60], *Desulfovibrio* had the highest abundance but lowest diversity among all of the rust layers. The OL had the most bacterial diversity, which may have been due to its close contact with the seawater.

Laboratory study of *D. bizertensis* SY-1 separated from the rust layers

The typical corrosion microorganism SRB in the rust layers was isolated and cultured. When the rust layer was inoculated into an anaerobic solid agar culture medium, the SRB were separated and concentrated. During the first two days after the inoculation in Postgate's culture (PGC) medium containing lactate as a carbon source, the culture solution became black. This revealed that iron sulfide was formed when the iron oxide in the rust reacted with the hydrogen sulfide created by the SRB. After 7 days of incubation at 30 °C, the color of the culture became darker (Fig. 6d). On the solid agar plates, round, black colonies with diameters of 3–5 mm grew, representing the SRB growth in the medium (Fig. 6c).

16S rDNA sequencing is not only conservative but also highly variable, so it is widely used in bacterial taxonomy[16,61]. This SRB strain was identified as *Desulfovibrio bizertensis* (98% similarity) and *Desulfovibrio singaporenus* (98% similarity) through 16S rDNA gene sequencing (Fig. 6g). According to the phylogenetic relationship, this strain of bacteria was named *Desulfovibrio bizertensis* SY-1.

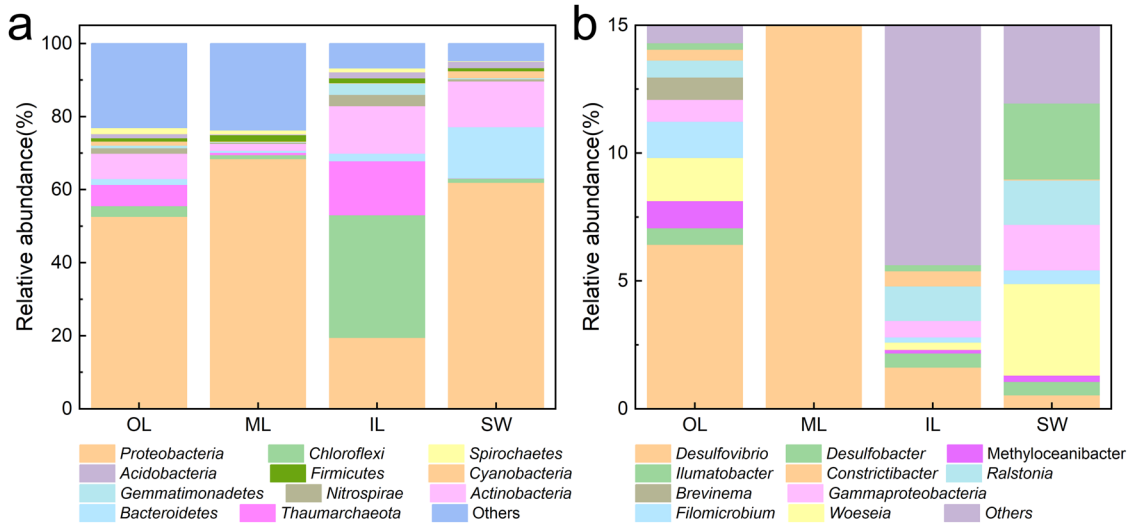

Fig. 5 Relative abundances of bacterial 16S rRNA gene sequences in the three-rust-layer corrosion products of Q345 steel. a Phylum and **b** genera level. OL outer rust layer rust, ML middle rust layer, IL inner rust layer, SW seawater.

Table 3. Relative abundance of bacterial 16S rRNA gene sequences obtained from rust and seawater samples at the genus level (%).

Genera	OL	ML	IL	SW
Desulfovibrio	6.43	37.43	1.63	0.54
Desulfobacter	0.64	6.69	0.55	0.53
Methyloceanibacter	1.06	1.59	0.13	0.24
Woeseia	1.69	0.21	0.29	3.58
Filomicrobium	1.42	0.65	0.21	0.54
Gammaproteobacteria	0.86	0.11	0.64	1.78
Brevinema	0.87	0.53	0	0
Ralstonia	0.66	0.4	1.35	1.73
Constrictibacter	0.43	0.03	0.59	0.04
Ilumatobacter	0.25	0.09	0.24	2.97
Others	85.69	52.27	94.37	88.05

A series of physiological metabolism tests revealed that this strain is a type of SRB (Fig. 7). *Desulfovibrio* was also the dominant genera in all of the rust layers (Table 3). The transmission electron microscopy (TEM) images of the microstructure of the SY-1 strain are presented in Fig. 6a, b, and the length of the cell shown is about 2–4 μm.

The surface morphologies of the carbon steel exposed to the SY-1 strain for 15 days are shown in Fig. 5e, f. Owing to its net-like structure, the homogeneity and looseness of the biofilm were apparent. More crowded cells and polysaccharides with a defined structure and a smooth surface can be identified in Fig. 5f. The SY-1 strain also produced an iron sulfide corrosion product layer with visible spherical granules.

The generation of H_2S by SRB, particularly those in the *Desulfovibrio* genus, was a significant factor in the MIC. The H_2S altered the environment's pH, resulting in the creation of FeS. *D. caledoniensis*[62], *D. vulgaris*[63], *D. vietnamensis*[64], and other *Desulfovibrio* strains isolated from rust layers have been shown to have severe corrosion abilities, which has been demonstrated in laboratory tests. In addition, the ability of some SRB species to degrade alkanes and aromatic hydrocarbons utilizing Fe^{3+} as the ultimate electron acceptor has been shown to be a characteristic that is significant to metal corrosion[37,38,65].

To analyze the growth curve of the planktonic SY-1 strain, the OD_{600} value of the culture medium was evaluated. Figure 7a presents the typical three-stage curve, and exponential development occurred during the first five days. The culture medium became rather turbid due to the fast expansion of the cells and its metabolites. The number of SY-1 cells reached the maximum value on the fifth day, and the cell concentration was about 10^8 cells/mL based on direct counting under a microscope. After this, the cell growth slowed down and came to a standstill.

Figure 7b shows that the pH values of the SRB media were nearby neutral. During the 15 days, the SRB culture medium increased sharply in the first 9 days, but it decreased during the last 6 days. The sulfate reduction by the SRB in the normal metabolism used H^+, which was obtained through organic carbon oxidation. In most cases, the total procedure resulted in no net change in the scalar or vector proton concentrations. Zhou et al.[66] reported similar findings. The SO_4^{2-} values were also determined (Fig. 7c). In the medium containing the SY-1 strain, the change in the SO_4^{2-} levels mirrored the change in the OD_{600}. The SO_4^{2-} was rapidly consumed by the fast development of the planktonic SY-1 cells in the first three days, after which the SO_4^{2-} concentration stabilized.

Above all, the SY-1 strain was a strictly anaerobic bacterium. This strain grew rapidly to reach the highest value in the first three days, while the sulfate in the culture solution was rapidly consumed. Moreover, the pH in the culture medium remained neutral throughout the process. Wang et al.[67] reported similar findings, indicating that H_2S does not contribute much to the corrosion of carbon steel at a neutral pH.

Corrosion rate tests on *D. bizertensis* SY-1

To evaluate the corrosion capacity of the SY-1 strain, the corrosion characteristics of the Q235 coupons induced by SY-1 and a typical well-known corrosive SRB, *Desulfovibrio caledoniensis*[35], were tested via electrochemical tests, weight loss tests, and pit depth measurements and the results were compared.

The MIC process is a bio-electrochemical process[25], so the electrochemical measurements and analyses revealed the corrosion influence of the SY-1 strain. The linear polarization resistance (LPR) measurements were performed on the coupons in sterile, SY-1 strain, and *D. caledoniensis* inoculated culture media after various periods of time (Fig. 8a). The R_p value in the sterile medium coupons increased in the first three days, indicating that the corrosion rate decreased with time. Similarly, Qiang et al.[68] previously reported this phenomenon. After three days, the R_p value started to decrease, indicating that the corrosion rate had increased. However, it decreased continuously in both types of SRB medium during the 15 days of immersion, indicating an

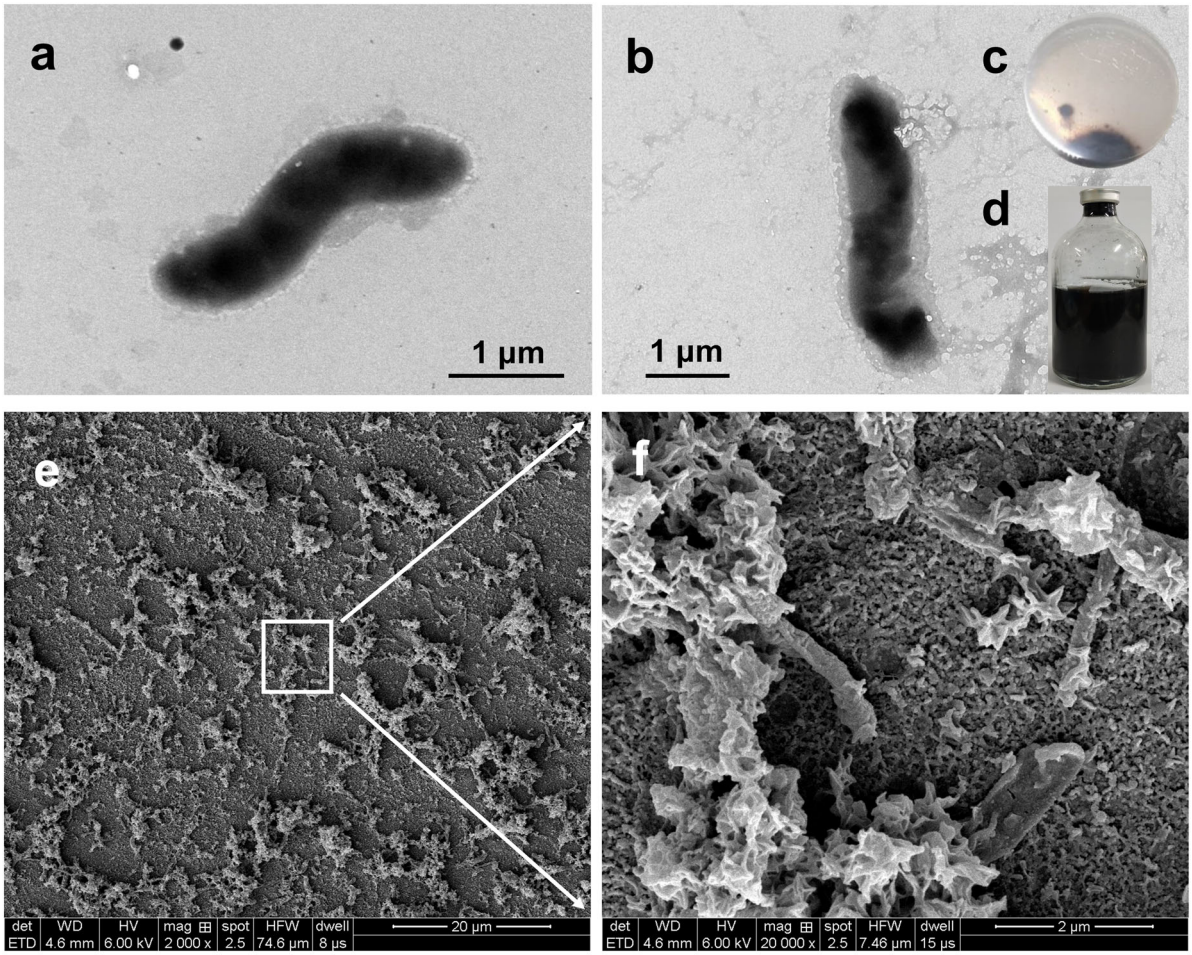

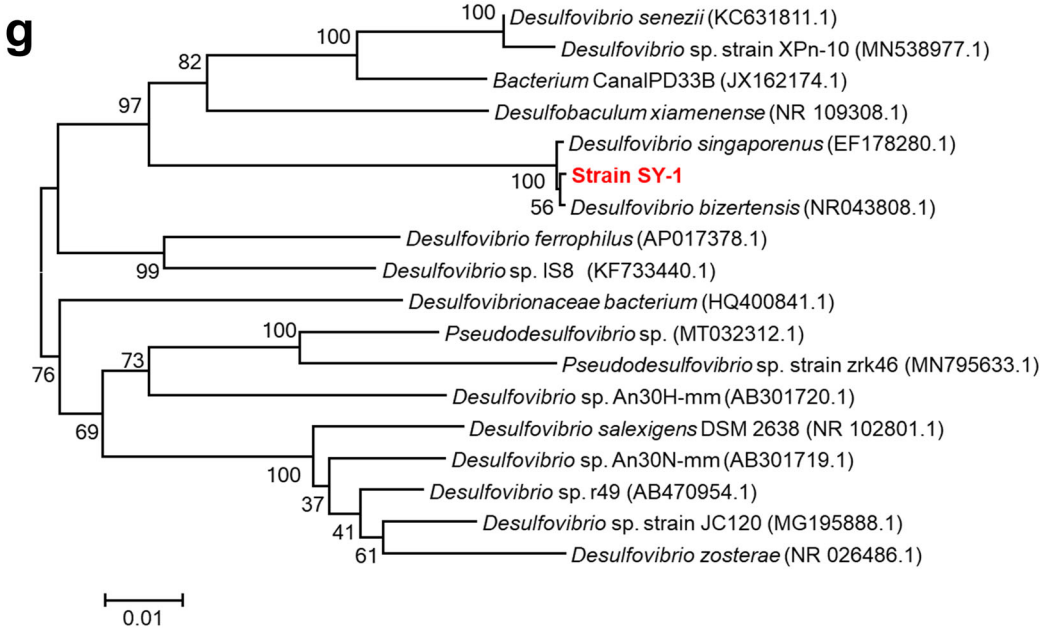

Fig. 6 Isolation and cultivation of *D. bizertensis* SY-1 from the rust layers. a, **b** TEM images of SY-1 strain, **c**, **d** optical images of SY-1 strain on solid agar plates and in liquid medium, **e**, **f** SEM images of the corrosion products of Q235 exposed in SY-1 media for 15 days, and **g** phylogenetic relationship between the 16S rDNA sequences from the SY-1libraries.

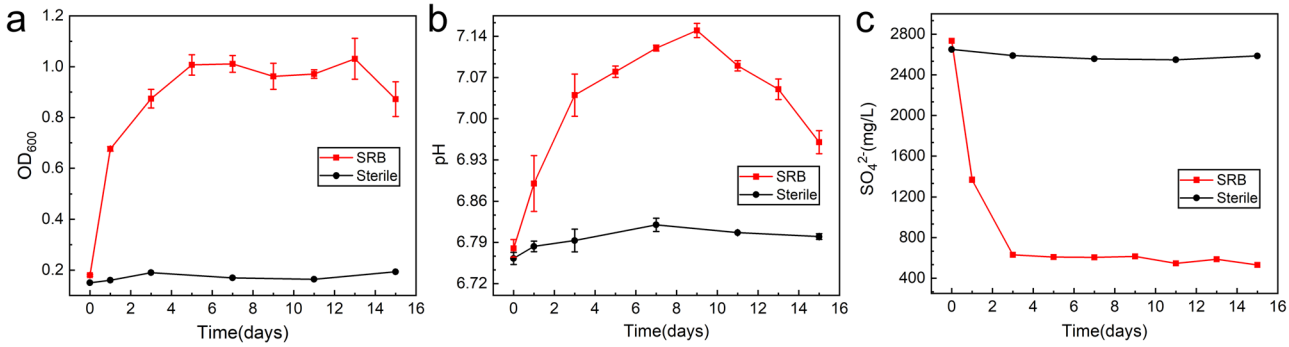

Fig. 7 Growth process of *D. bizertensis* SY-1 strain. a Growth curve, **b** pH, and **c** SO_4^{2-} values of the Q235 coupons in the sterile and SY-1 inoculated culture media after different days (error bars stand for the standard deviations from three independent sample).

increase in the corrosion rate. Although the FeS layers may have inhibited the carbon steel corrosion, the SRB biofilm had a considerably greater corrosion-promoting impact, which may have resulted in fast carbon steel degradation. A comparison of the LPR results for these two strains revealed that the R_p values in the SY-1 strain medium were much lower than those of the *D. caledoniensis* medium.

Figure 8b shows the potentiodynamic polarization curves for the various media after 15 days of exposure. The corrosion current density of the SY-1 strain (22.6 μA/cm^2) was nearly seven times higher than that of the sterile medium (2.9 μA/cm^2) and almost three times higher than that of the *D. caledoniensis* culture medium (6.5 μA/cm^2). The presence of the SY-1 strain considerably increased the corrosion rate of the carbon steel according to these findings.

To exactly determine the corrosion capacity of the SY-1 strain, the weight loss of the coupons was measured. Some typical SRB corrosion rates are also given in Fig. 8c to help compare the SY-1 strain's corrosion rate. Although there were differences in the compositions of the media used for the different SRB, the weight loss tests were similar, and the comparison of the corrosion abilities of the different SRB also has a certain value. The weight loss of the Q235 steel in the SY-1 medium after 15 days of exposure was 13.561 ± 2.89 mg/cm^2, and its corrosion rate was four times that in the sterile cultured medium. Based on the other SRB corrosion data[63,69–72], the carbon steel coupons in the SY-1 strain medium experienced a larger corrosion weight loss than those due to the other SRB, and the corrosion rate of the SY-1 strain was more than one third higher than that of the more corrosive *D. desulfuricans*.

Figure 8d shows the pitting morphologies of the carbon steel under different culture conditions after separating the corrosion products. During the 15 days of exposure to anaerobic and sterile conditions, no apparent corrosion pits formed on the coupon surfaces. The different SRB produced different forms of corrosion. After the 15 days of exposure, the carbon steel coupons in the *D. caledoniensis* medium exhibited uniform corrosion morphologies. However, in the SY-1 strain medium, the coupon's surface exhibited substantially more severe localized corrosion morphologies. Figure 8d shows that the greatest pit depth created by the SY-1 biofilms was 43.769 μm, which was approximately four times higher than that in the *D. caledoniensis* medium (10.027 μm). These results demonstrate that the SY-1 strain dramatically aggravated the localized corrosion.

Schematic of the rust layer structure

Electrochemical reactions between the atoms on the coupon surface and the ions/atoms in the seawater would cause corrosion, hence the microstructure of the corrosion layers would change over time under long-term seawater immersion and the activities of corrosion microorganisms[22,39,73].

For Q345 carbon steel immersed for 5.5 years in the South China Sea, specific corrosion products gradually evolved following the proposed corrosion mechanism (Fig. 9). Three distinct layers were identified: an inner rust layer, a thick intermediate layer, and an outer rust-biofilm layer. The rust layers and the microorganisms living in them strongly affected each other. The microorganisms had a substantial impact in the rust layer formation process, and the rust layers also exhibited the major effects of their different microbial communities.

When initially immersed in seawater, the carbon steel suffered from the severe corrosive environment, forming primal corrosion products. Meanwhile, marine microorganisms also adhered to the surface of the steel. The dissolved oxygen species might have reacted with the Fe^{2+}, with Reaction (1) occurring at the anode and Reaction (2) occurring at the cathode.

$$Fe \rightarrow Fe^{2+} + 2e^{-}. \quad (1)$$

$$O_2 + 2H_2O + 4e^{-} \rightarrow 4OH^{-}. \quad (2)$$

This could take place via Reaction (3):

$$2Fe + O_2 + 2H_2O \rightarrow 2Fe(OH)^{+} + 2OH^{-}. \quad (3)$$

Because the $Fe(OH)^{+}$ ions were unstable, they could further combine with O_2 to generate an FeOOH film[55]:

$$4Fe(OH)^{+} + 4OH^{-} + O_2 \rightarrow 4\beta - FeOOH + 2H_2O; \text{or} \quad (4)$$

$$4Fe(OH)^{+} + 4OH^{-} + O_2 \rightarrow 4\gamma - FeOOH + 2H_2O. \quad (5)$$

Green rust formed near the steel layer[42,74]:

$$5Fe(OH)_2 + Fe^{2+} + 1/2O_2 + 9H_2O + SO_4^{2-} \rightarrow GR. \quad (6)$$

Subsequently, the dehydration reaction γ-FeOOH → γ-Fe_2O_3 occurred to form a stable iron oxide[55]. These substances were detected in the ML via XRD and Raman spectroscopy. The excess positive charge and acidity were increased by the Fe^{2+} hydrolysis, which occurred in anodic areas at the steel/rust interface. According to the XPS results, the extra positive charge at the steel/rust interface attracted the Cl^{-} and SO_4^{2-} ions in the seawater, resulting in greater chlorinity in the rust layers (Table 1). The high sulfate content may have facilitated the formation of green rust near the surface of the steel.

γ-FeOOH would be also reduced to Fe_3O_4 by Fe^{2+} through the following reaction[75]:

$$2\gamma - FeOOH + Fe^{2+} \rightarrow Fe_3O_4 + 2H^{+}. \quad (7)$$

In addition, Fe_3O_4 can also be directly formed from metals in an oxygen-deficient environment[45].

$$3Fe + 4H_2O \rightarrow Fe_3O_4 + 4H_2. \quad (8)$$

Therefore, Fe_3O_4 was abundantly present in the IL, and it was also detected in the ML and OL.

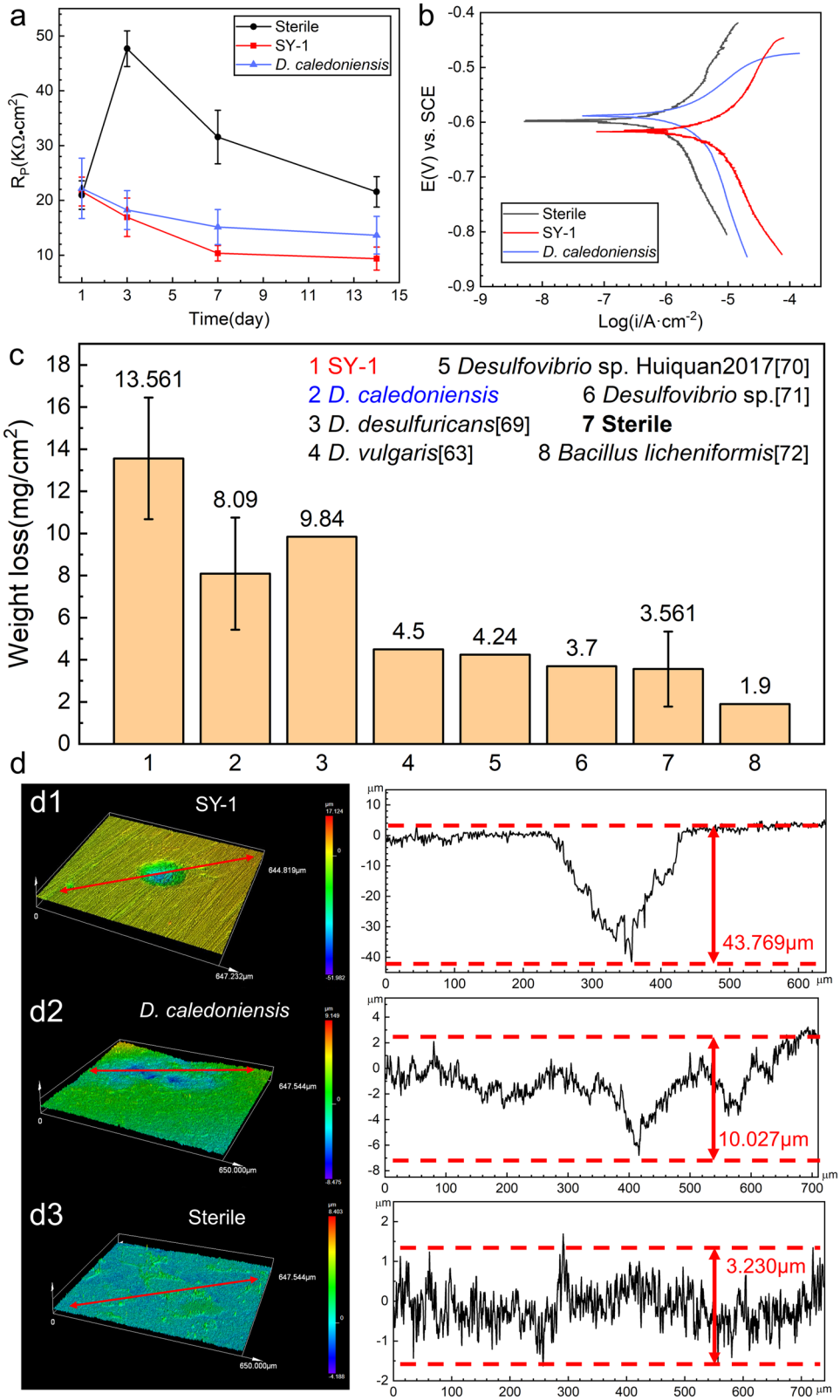

Fig. 8 Corrosion rate tests on *D. bizertensis* SY-1. a LPR, **b** potentiodynamic polarization curves, **c** weight loss, and **d** CLSM images of the Q235 coupons in the sterile, SY-1 strain, *D. caledoniensis* inoculated culture media after 15 days (error bars stand for the standard deviations from three independent sample).

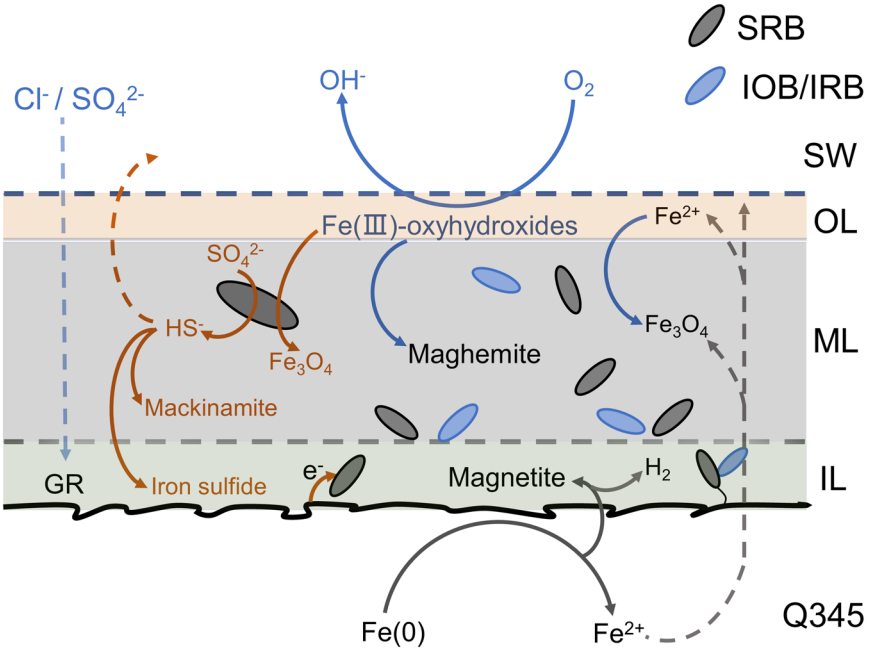

Fig. 9 Schematic diagram of the major corrosion products for Q345 carbon steel in a long-time seawater corrosion. Under the influences of these complex microbial communities and the marine environment, three relatively stable rust layers were formed. Magnetite (Fe_3O_4) and small amounts of iron sulfide and green rust were identified in the IL. The ML was predominantly composed of maghemite (γ-Fe_2O_3), together with Fe3O4 and mackinamite. The OL contained Fe(III)-oxyhydroxides (α-FeOOH and γ-FeOOH), along with a large number of fouling organisms attached to the surface. In all of the rust layers, anaerobic SRB were found to play an important role in the formation of the corrosion products.

Microorganisms also played an important role in the formation process of the corrosion products. The microorganisms in seawater would utilize these minerals to support their own survival and metabolism as the rust layer grew. The formation of iron oxides and the consumption of oxygen by the aerobic bacteria in the rust layer may have supported the growth of and metabolism the SRB as well. As is shown in Fig. 5 and Table 3, the anaerobic SRB became the dominant bacteria in all of the rust layers. As has been previously reported, the SRB always utilized sulfate as the terminal electron acceptor, eventually converting it to HS^-[76].

$$SO_4^{2-} + 9H^+ + 8e^- \rightarrow HS^- + 4H_2O. \quad (9)$$

$$2FeOOH + 3HS^- + 3H^+ \rightarrow 2FeS + S + 4H_2O. \quad (10)$$

The HS^- reacted with the Fe^{2+} produced by the metal dissolution to form FeS. Some of the HS^- generated by the SRB diffused into the seawater, while the rest of it accumulated on the surface of the steel because the metal surface acted as an anode (1). The IL had the highest HS^- content among the three layers, while the HS^- contents of the ML and OL were lower than that of the IL (Table 2).

Near the surface of the steel, the IL was a steel-surface-connected electronic conductor, which was mainly composed of magnetite and a small amount of iron sulfide. Some of the SRB may have obtained electrons directly from the steel's surface through direct electron transfer (DET)[34]. Zhang et al.[18] found that the dominant community in the inner rust layer of carbon steel was mainly *Desulfovibiro*, which can directly transfer electrons. Electroactive SRB can also sustain their long survival by utilizing the Fe_3O_4/FeS particle network attached to the metal surface[45]. In addition, the H_2 produced during the formation of Fe_3O_4 (Reaction (8)) may have also been utilized by the SRB or hydrogen-consuming microorganisms. The carbon steel could have served as a cathodic zone, while the SRB acted as the cathode region. Thus, although the IL was basically considered to be an anaerobic environment, the carbon steel corrosion would still be aggravated. The Fe^{2+} and H^+ generated in the IL would diffuse into the ML, which would further promote the corrosion of the ML and increase the thickness of the ML.

After long-term immersion, previous studies[77–79] have found that ferric oxide can act as an electron acceptor and can be easily reduced via microbial metabolism in anaerobic environments. Wei et al.[60] also reported that SRB can use not only sulfate ions but also ferric hydroxide as electron acceptors to acquire energy for their growth. FeOOH can be converted into Fe_3O_4 under the action of SRB. In this study, it was found that the ML contained a large amount of γ-Fe_2O_3, which may be due to the γ-FeOOH dehydration reaction. The XRD and Raman results also revealed that the ML was predominantly composed of maghemite and only a small amount of magnetite (Fig. 3).

A large number of fouling organisms, such as diatoms and corals, colonized the OL owing to its direct contact with the seawater (Fig. 2e, f). Marine biofouling is a complex natural phenomenon. Marine organisms in seawater can colonize and grow on the surface of the material to complete their life cycles and form a fouling biological community that adapts to the environment. Under the influence of these biological communities, the iron oxide would be further oxidized and fall off. Under the influence of such a complex microbial community in a marine environment, three relatively stable rust layers were formed.

Moreover, aerobic bacteria such as *Filomicrobium* and *Ruegeria* were also the dominant microorganisms in all of the rust layers. They also played key roles in the formation of the corrosion products, and they could form an anoxic and acidic environment in the rust layers and produce extracellular polymeric substance (EPS). For example, *Methyloceanibacter* was the dominant aerobic microorganism in all of the rust layers, and this organism is a methylotroph that consumes methanol, methylamine, trimethylamine, and a range of other multi-carbon chemicals[80].

Therefore, the IL and ML were formed under the influence of SRB. Previous studies have found[8,45] that under actual seawater

immersion, the black corrosion products in the IL were mainly magnetite and green rust, and the orange-brown corrosion products in the OL were mainly Fe(III)-oxyhydroxides with a small amount of maghemite. In this study, the IL layer was mainly composed of magnetite, as well as small amounts of iron sulfide and green rust, so the electroactive SRB may have directly obtained electrons from the iron surface and utilized the Fe_3O_4/FeS particle network to survive persistently. The ML was mainly composed of γ-Fe_2O_3 and small amounts of magnetite and mackinamite due to the FeOOH dehydration reaction and the SRB activity.

The SRB were the dominant bacteria in all rust layers, but the proportions were quite different. The SRB were the most abundant in the ML (accounting for up to 44%) due to the diffusion of seawater and the nutrients produced by the biofouling in the OL, which supplied sufficient electron donors and acceptors for the SRB. The SRB accounted for 6% in the OL, i.e., less than in the ML. Through high-throughput sequencing, Zhang et al.[18] also found that the dominant bacteria in the OL of carbon steel rust were SRB that could produce spores. Previous study also found the number of SRB could reach 10^4 CFU/g in the steel rust layer[17].

The SRB were the least abundant (only 2%) in the IL despite the presence of an appropriate anaerobic environment due to the lack of energy supplying substances (which were consumed by the SRB in the ML) (Table 2).

Overall, the interactions between microorganisms and the rust layers strongly affected each other. With the formation of iron minerals, the microorganisms would use these minerals to promote their own growth and metabolism. Under the influence of the EPS secreted by some of the key microorganisms, specific corrosion products, such as iron sulfide, were also formed in the rust layers. The results of this study indicate that although SRB were determined to be the most important microbial corrosive bacteria, many highly corrosive SRB have still not been cultivated, and their corrosion behavior still needs to be studied.

METHODS

Materials

Q345 specifications (wt.%: C 0.20, Si 0.55, Mn 1.70, S 0.005, P 0.04, and V 0.08) of 40 × 20 × 5 mm was employed in this study. The coupons were ground with a series of grit (#240 and #400) SiC papers, and followed by rinsed with deionized water. Subsequently, these coupons immersed in ethanol for degreasing, and dried immediately. The coupons (three parallel samples) were fixed in insulating plastic frames and exposed to seawater at a depth of 1 m below sea level in the coastal zone of Hongtang Bay (18°17'58″ N, 109°15'18″ E), in Sanya, Hainan Province, China. Each coupon was exposed for 5.5 years from June 2014 to December 2019.

After 5.5 years of immersion, the rust layers were sampled and analyzed (Fig. 1a). The different rust layers were mainly delineated based on the macroscopic colors and textures of the corrosion products. The cross-sections of the Q345 coupons (Fig. 1) contained three distinct layers based on the colors: a dark-green innermost layer (referred to as IL, ~1 mm thick), a black second/middle layer (referred to as ML, ~8–10 mm thick), and a grey and red outermost layer (referred to as OL, ~2–3 mm thick). A sterile scalpel was used to very carefully perform the dissection, and then, the sample was laced in an anaerobic bag and sealed to prevent the corrosion products from being oxidized. When taking the samples of the different rust layers, a new sterile scalpel blade was used to sample each layer.

Characterization of the rust layers

For SEM analysis, the samples were preserved in a glutaraldehyde solution of 2.5% (v/v). A scanning electron microscope/energy dispersive X-ray detector (SEM/EDS, FEI Quanta 250) with an accelerating voltage of 6–20 kV was used to examine the morphologies of rust layers and evaluate its elements. Coupons were dehydrated with 25, 50, 70, 80, and 100% ethanol (v/v) for 10 min at each concentration, and then sputter coated with Au.

The crystal structures of the rust layers were studied using an X-ray diffraction (XRD, Rigaku D/max-Ultima IV) under the following conditions: Cu Karadiation (=0.1542 nm), 40 kV, 30 mA.

A laser Raman spectroscopy (Raman, HORIBA Jobin Yvon) operated with a green Nd: YAG laser (532 nm) was used. To minimize sample deterioration by laser heating, the laser power was maintained low, approximately 1 mW. To study the organic components in the rust layers, Fourier transform infrared spectra (FT-IR, Thermo Nicolet iS10) were used. An X-ray photoelectron spectroscopy (XPS, ESCALAB 250XI) was also used to analyze the valence state of C, Fe, O, and S elements. The photoelectrons were driven by an Al Ka (1486.6 eV) X-ray source with a 50.0 eV analyzer pass energy. The surface carbon contamination was used to calibrate binding energies (BEs) at 284.6 eV.

The DNA from rust layer and sea water samples were extracted using a previously reported method[18].

Isolation of SRB

Sterile scalpel was used to transfer the inner rust layer directly into the sterile PGC media[35]. The medium consisted of (g L^{-1}): yeast extract 1.0, tri-sodium citrate 0.3, sodium lactate 6.7, $CaCl_2{\cdot}6H_2O$ 0.06, NH_4Cl 1.0, $MgSO_4$ 0.06, $Fe(NH_4)_2(SO_4)_2$ 1.0, and KH_2PO_4 0.5 in sea water. The pH of the culture medium was adjusted to 7.2 using NaOH. Then the inoculated media were cultured at 30 °C for 72 h. After the media turned black, the isolation and cultivation procedure of anaerobic bacteria was performed following ref. [35]. The obtained SRB colonies were further preserved in liquid PGC media at 4 °C and as anaerobic bacteria preservation solution stocked at −80 °C.

According to the identification, this isolated and cultured SRB strain was named as *Desulfovibrio bizertensis* SY-1 (as shown in Fig. 6 in section 3.3.1). Transmission electron microscopy (TEM, JEM-1200EX) was used to analyze the morphologies of the SY-1 strain. Copper meshes were placed in SRB cultured media that had been pre-treated for 2 h. with 2.5% glutaraldehyde. The copper meshes were then dried under infrared light conditions and examined under a TEM.

Exposure tests with SY-1 strain

The corrosion weight loss tests on the Q235 carbon steel (AISI 1018) were conducted in 100 mL anaerobic vials to study the corrosion ability of the SY-1 strain. Q235 carbon steel coupons (10 × 10 × 3 mm in size) were ground using abrasive paper (#800, #1200, and #2000) and were ultrasonically cleaned in ethanol. Before use, the coupons were dried with N_2 and then irradiated under UV light for 20 min to sterilize them.

An inoculum of 0.5 mL (1% v/v) of 5-day-old SY-1 planktonic culture was added to 50 mL of sterile culture medium containing a sterilized Q235 coupon. After the inoculation, each anaerobic vial was incubated at 30 °C for 360 h.

The optical density (OD) method at 600 nm was used to determine the growth curve of the SY-1 strain[68]. The concentration of SO_4^{2-}, which reflected the SRB metabolic activity, was also analyzed using an ion chromatography system (IC, 883 Basic IC plus). A pH meter (pH, METTLER TOLEDO S220-B) was used to determine the culture medium's pH level. The pH and OD_{600} samples were recorded for three separate trials.

To evaluate the corrosiveness of the SY-1 strain, a commonly used *Desulfovibrio caledoniensis* strain was also analyzed for comparison. After 360 h of exposure, the surface morphologies of the Q235 coupons were observed via SEM. Before exposure, the

mass of each cleaned and sterilized Q235 coupon was recorded using an electronic balance (precision ± 0.1 mg).

After exposure, the carbon steel coupons were cleaned using a de-rusting solution (ISO 8501:2009, IDT) for at least 3 min to eliminate the corrosion products. Deionized water and ethanol were used to clean the coupons. Then, N_2 was used to dry the coupons, and each coupon's weight was measured. Each group contained a set of three samples. The number, diameter, and depth of the corrosion pits on the corroded coupons were determined via confocal laser scanning microscopy (CLSM, Lext OLS5000).

Electrochemical measurements

The electrochemical measurements were performed in the sterile, SY-1 strain and *D. caledoniensis* inoculation medium at 30 °C using an electrochemical station (Gamry, Reference 3000). A typical three-electrode system was used for testing, in which a Q235 coupon as the working electrode, platinum as the counter electrode, and a saturated calomel electrode (SCE) as the reference electrode. The linear polarization resistance (LPR) and potentiodynamic polarization curves were both measured. To guarantee the accuracy of the measurements, the open circuit potential (OCP) was tested for at least 20 min to ensure system stability. EIS parameters were consistent with Qian et al.[68]. The potentiodynamic polarization curves were performed with a scanning rate of 0.5 mV/s after the 14-day exposed tests, and the scanning potential range was from −250 to +250 mV vs. OCP. Electrochemical experiments were carried out on three separate sets of samples ($n = 3$).

DATA AVAILABILITY

All data needed to evaluate the conclusions in the paper are present in the paper and/or the Supplementary Materials. 16S amplicon sequence files are available at the NCBI Sequence Read Archive under accession numbers PRJNA790473 for SY-1 strain. Additional data related to this paper are available from the corresponding author upon reasonable request.

Received: 16 June 2022; Accepted: 25 October 2022;
Published online: 11 November 2022

REFERENCES

1. Li, X. et al. Analysis of bacterial community composition of corroded steel immersed in Sanya and Xiamen seawaters in China via method of Illumina MiSeq sequencing. *Front. Microbiol.* **8**, 1737 (2017).
2. Hou, B. et al. The cost of corrosion in China. *npj Mater. Degrad.* **1**, 4 (2017).
3. Li, S., George, R. D. & Hihara, L. H. Corrosion analysis and characteristics of discarded military munitions in ocean waters. *Corros. Sci.* **102**, 36–43 (2016).
4. Refait, P., Grolleau, A.-M., Jeannin, M., François, E. & Sabot, R. Corrosion of mild steel at the seawater/sediments interface: Mechanisms and kinetics. *Corros. Sci.* **130**, 76–84 (2018).
5. Ma, A. L., Jiang, S. L., Zheng, Y. G. & Ke, W. Corrosion product film formed on the 90/10 copper–nickel tube in natural seawater: Composition/structure and formation mechanism. *Corros. Sci.* **91**, 245–261 (2015).
6. Rémazeilles, C., Lévêque, F., Conforto, E. & Refait, P. Long-term alteration processes of iron fasteners extracted from archaeological shipwrecks aged in biologically active waterlogged media. *Corros. Sci.* **181**, 109231 (2021).
7. Melchers, R. E., Jeffrey, R. J. & Usher, K. M. Localized corrosion of steel sheet piling. *Corros. Sci.* **79**, 139–147 (2014).
8. Refait, P., Grolleau, A.-M., Jeannin, M., François, E. & Sabot, R. Localized corrosion of carbon steel in marine media: Galvanic coupling and heterogeneity of the corrosion product layer. *Corros. Sci.* **111**, 583–595 (2016).
9. Ingo, G. M. et al. Micro-chemical investigation of corrosion products naturally grown on archaeological Cu-based artefacts retrieved from the Mediterranean sea. *Appl. Surf. Sci.* **470**, 695–706 (2019).
10. Smith, M. Accelerated low water corrosion: The microbial sulfur cycle in microcosm. *npj Mater. Degrad.* **37**, 1–11 (2019).
11. Xu, L. et al. Inadequate dosing of THPS treatment increases microbially influenced corrosion of pipeline steel by inducing biofilm growth of *Desulfovibrio hontreensis* SY-21. *Bioelectrochemistry* **145**, 108048 (2022).
12. Tuck, B., Watkin, E., Somers, A. & Machuca, L. L. A critical review of marine biofilms on metallic materials. *npj Mater. Degrad.* **6**, 25 (2022).
13. Huttunen-Saarivirta, E. et al. Microbiologically influenced corrosion (MIC) in stainless steel heat exchanger. *Appl. Surf. Sci.* **258**, 6512–6526 (2012).
14. Little, B. J., Hinks, J. & Blackwood, D. J. Microbially influenced corrosion: Towards an interdisciplinary perspective on mechanisms. *Int. Biodeterior. Biodegrad.* **154**, 105062 (2020).
15. Cybulska, K., Łońska, E. & Fabisiak, J. Bacterial benthic community composition in the Baltic Sea in selected chemical and conventional weapons dump sites affected by munition corrosion. *Sci. Total Environ.* **709**, 136112 (2020).
16. Kotu, S. P., Mannan, M. S. & Jayaraman, A. Emerging molecular techniques for studying microbial community composition and function in microbiologically influenced corrosion. *Int. Biodeterior. Biodegrad.* **144**, 104722 (2019).
17. Li, X. et al. Analysis of cultivable aerobic bacterial community composition and screening for facultative sulfate-reducing bacteria in marine corrosive steel. *J. Ocean. Limnol.* **37**, 600–614 (2019).
18. Zhang, Y. et al. Analysis of marine microbial communities colonizing various metallic materials and rust layers. *Biofouling* **35**, 429–442 (2019).
19. Huttunen-Saarivirta, E., Rajala, P., Bomberg, M. & Carpén, L. Corrosion of copper in oxygen-deficient groundwater with and without deep bedrock micro-organisms: Characterisation of microbial communities and surface processes. *Appl. Surf. Sci.* **396**, 1044–1057 (2017).
20. Chu, Y., Xu, P., Ou, Y., Bai, P. & Wei, Z. Corrosion behavior and interaction of mixed bacteria on carbon steel in reclaimed water. *Sci. Total Environ.* **718**, 136679 (2020).
21. Marks, C. R. et al. An integrated metagenomic and metabolite profiling study of hydrocarbon biodegradation and corrosion in navy ships. *npj Mater. Degrad.* **5**, 60 (2021).
22. Jeffrey, R. & Melchers, R. E. Bacteriological influence in the development of iron sulphide species in marine immersion environments. *Corros. Sci.* **45**, 693–714 (2003).
23. Sun, H., Shi, B., Lytle, D. A., Bai, Y. & Wang, D. Formation and release behavior of iron corrosion products under the influence of bacterial communities in a simulated water distribution system. *Environ. Sci.: Process. Impacts* **16**, 576 (2014).
24. Wu, T., Sun, C., Yan, M., Xu, J. & Yin, F. Sulfate-reducing bacteria-assisted cracking. *Corros. Rev.* **37**, 231–244 (2019).
25. Gu, T., Jia, R., Unsal, T. & Xu, D. Toward a better understanding of microbiologically influenced corrosion caused by sulfate reducing bacteria. *J. Mater. Sci. Technol.* **35**, 631–636 (2019).
26. Guan, F. et al. Synergistic effect of carbon starvation and exogenous redox mediators on corrosion of X70 pipeline steel induced by Desulfovibrio singaporenus. *Sci. Total Environ.* **788**, 147573 (2021).
27. Zhang, Y. et al. Microbiologically influenced corrosion of steel in coastal surface seawater contaminated by crude oil. *npj Mater. Degrad.* **6**, 35 (2022).
28. Chen, S., Li, Y. & Cheng, Y. F. Nanopatterning of steel by one-step anodization for anti-adhesion of bacteria. *Sci. Rep.* **7**, 5326 (2017).
29. Javed, M. A., Neil, W. C., McAdam, G. & Wade, S. A. Effect of sulphate-reducing bacteria on the microbiologically influenced corrosion of ten different metals using constant test conditions. *Int. Biodeterior. Biodegrad.* **125**, 73–85 (2017).
30. Javaherdashti, R. & Akvan, F. *Failure Modes, Effects and Causes of Microbiologically Influenced Corrosion* 43–104 (Elsevier, 2020).
31. Little, B. J. et al. Microbially influenced corrosion—Any progress? *Corros. Sci.* **170**, 108641 (2020).
32. Deng, X., Saito, J., Kaksonen, A. & Okamoto, A. Enhancement of cell growth by uncoupling extracellular electron uptake and oxidative stress production in sediment sulfate-reducing bacteria. *Environ. Int.* **144**, 106006 (2020).
33. Dinh, H. T. et al. Iron corrosion by novel anaerobic microorganisms. *Nature* **427**, 829 (2004).
34. Li, Y. et al. Anaerobic microbiologically influenced corrosion mechanisms interpreted using bioenergetics and bioelectrochemistry: A review. *J. Mater. Sci. Technol.* **34**, 1713–1718 (2018).
35. Duan, J. et al. Corrosion of carbon steel influenced by anaerobic biofilm in natural seawater. *Electrochim. Acta* **54**, 22–28 (2008).
36. Tang, H.-Y. et al. Stainless steel corrosion via direct iron-to-microbe electron transfer by Geobacter species. *ISME J.* **15**, 3084–3093 (2021).
37. Musat, F. et al. Anaerobic degradation of naphthalene and 2-methylnaphthalene by strains of marine sulfate-reducing bacteria. *Environ. Microbiol.* **11**, 209–219 (2009).
38. Kniemeyer, O. et al. Anaerobic oxidation of short-chain hydrocarbons by marine sulphate-reducing bacteria. *Nature* **449**, 898–901 (2007).

39. Beech, I. B. & Campbell, S. A. Accelerated low water corrosion of carbon steel in the presence of a biofilm harbouring sulphate-reducing and sulphur-oxidising bacteria recovered from a marine sediment. *Electrochim. Acta* **54**, 14–21 (2008).
40. Li, S. & Hihara, L. H. A micro-Raman spectroscopic study of marine atmospheric corrosion of carbon steel: The effect of akaganeite. *J. Electrochem. Soc.* **162**, C495–C502 (2015).
41. Morcillo, M. et al. SEM/micro-Raman characterization of the morphologies of marine atmospheric corrosion products formed on mild steel. *J. Electrochem. Soc.* **163**, C426–C439 (2016).
42. Refait, P. et al. Electrochemical formation of green rusts in deaerated seawater-like solutions. *Electrochim. Acta* **56**, 6481–6488 (2011).
43. Rémazeilles, C. et al. Mechanisms of long-term anaerobic corrosion of iron archaeological artefacts in seawater. *Corros. Sci.* **51**, 2932–2941 (2009).
44. Refait, P., Memet, J.-B., Bon, C., Sabot, R. & Génin, J.-M. R. Formation of the Fe(II)–Fe(III) hydroxysulphate green rust during marine corrosion of steel. *Corros. Sci.* **45**, 833–845 (2003).
45. Refait, P., Grolleau, A.-M., Jeannin, M., Rémazeilles, C. & Sabot, R. Corrosion of carbon steel in marine environments: Role of the corrosion product layer. *CMD* **1**, 198–218 (2020).
46. Bao, Q., Zhang, D., Lv, D. & Wang, P. Effects of two main metabolites of sulphate-reducing bacteria on the corrosion of Q235 steels in 3.5wt.% NaCl media. *Corros. Sci.* **65**, 405–413 (2012).
47. Sheng, X., Ting, Y. P. & Pehkonen, S. O. The influence of ionic strength, nutrients and pH on bacterial adhesion to metals. *J. Colloid Interface Sci.* **321**, 256–264 (2008).
48. Liu, H., Gu, T., Asif, M., Zhang, G. & Liu, H. The corrosion behavior and mechanism of carbon steel induced by extracellular polymeric substances of iron-oxidizing bacteria. *Corros. Sci.* **114**, 102–111 (2017).
49. Mullet, M., Guillemin, Y. & Ruby, C. Oxidation and deprotonation of synthetic FeII–FeIII (oxy)hydroxycarbonate Green Rust: An X-ray photoelectron study. *J. Solid State Chem.* **181**, 81–89 (2008).
50. de la Fuente, D. et al. Characterisation of rust surfaces formed on mild steel exposed to marine atmospheres using XRD and SEM/Micro-Raman techniques. *Corros. Sci.* **110**, 253–264 (2016).
51. Dubois, F., Mendibide, C., Pagnier, T., Perrard, F. & Duret, C. Raman mapping of corrosion products formed onto spring steels during salt spray experiments. A correlation between the scale composition and the corrosion resistance. *Corros. Sci.* **50**, 3401–3409 (2008).
52. Demoulin, A. et al. The evolution of the corrosion of iron in hydraulic binders analysed from 46- and 260-year-old buildings. *Corros. Sci.* **52**, 3168–3179 (2010).
53. Neff, D., Dillmann, P., Bellot-Gurlet, L. & Beranger, G. Corrosion of iron archaeological artefacts in soil: Characterisation of the corrosion system. *Corros. Sci.* **47**, 515–535 (2005).
54. Bourdoiseau, J.-A., Jeannin, M., Sabot, R., Rémazeilles, C. & Refait, P. Characterisation of mackinawite by Raman spectroscopy: Effects of crystallisation, drying and oxidation. *Corros. Sci.* **50**, 3247–3255 (2008).
55. Yang, J., Lu, Y., Guo, Z., Gu, J. & Gu, C. Corrosion behaviour of a quenched and partitioned medium carbon steel in 3.5 wt.% NaCl solution. *Corros. Sci.* **130**, 64–75 (2018).
56. Nishimura, T., Katayama, H., Noda, K. & Kodama, T. Electrochemical behavior of rust formed on carbon steel in a wet/dry environment containing chloride ions. *Corrosion* **56**, 935–941 (2000).
57. Morcillo, M. et al. Scanning electron microscopy/micro-Raman: A very useful technique for characterizing the morphologies of rust phases formed on carbon steel in atmospheric exposures. *Corrosion* https://doi.org/10.5006/2059 (2016).
58. Herman, R. G., Bogdan, C. E., Sommer, A. J. & Simpson, D. R. Discrimination among carbonate minerals by Raman spectroscopy using the laser microprobe. *Appl Spectrosc.* **41**, 437–440 (1987).
59. Castaneda, H. & Benetton, X. D. SRB-biofilm influence in active corrosion sites formed at the steel-electrolyte interface when exposed to artificial seawater conditions. *Corros. Sci.* **50**, 1169–1183 (2008).
60. Wei, B. Effect of sulfate-reducing bacteria on corrosion of X80 pipeline steel under disbonded coating in a red soil solution. *J. Mater. Sci.* **87**, 1–7 (2021).
61. de Sousa Pires, A. et al. Molecular diversity and abundance of the microbial community associated to an offshore oil field on the southeast of Brazil. *Int. Biodeterior. Biodegrad.* **160**, 105215 (2021).
62. Yu, L., Duan, J., Zhao, W., Huang, Y. & Hou, B. Characteristics of hydrogen evolution and oxidation catalyzed by Desulfovibrio caledoniensis biofilm on pyrolytic graphite electrode. *Electrochim. Acta* **56**, 9041–9047 (2011).
63. Zhang, P., Xu, D., Li, Y., Yang, K. & Gu, T. Electron mediators accelerate the microbiologically influenced corrosion of 304 stainless steel by the Desulfovibrio vulgaris biofilm. *Bioelectrochemistry* **101**, 14–21 (2015).
64. Tarasov, A. L. & Borzenkov, I. A. Sulfate-reducing bacteria of the genus Desulfovibrio from south vietnam seacoast. *Microbiology* **84**, 553–560 (2015).
65. Gu, T., Wang, D., Lekbach, Y. & Xu, D. Extracellular electron transfer in microbial biocorrosion. *Curr. Opin. Electrochem.* **29**, 100763 (2021).
66. Dou, W. et al. Investigation of the mechanism and characteristics of copper corrosion by sulfate reducing bacteria. *Corros. Sci.* **144**, 237–248 (2018).
67. Wang, D. et al. Distinguishing two different microbiologically influenced corrosion (MIC) mechanisms using an electron mediator and hydrogen evolution detection. *Corros. Sci.* **177**, 108993 (2020).
68. Qian, H. et al. Laboratory investigation of microbiologically influenced corrosion of Q235 carbon steel by halophilic archaea Natronorubrum tibetense. *Corros. Sci.* **145**, 151–161 (2018).
69. Li, X. & Sun, C. Synergistic effect of carbamide and sulfate reducing bacteria on corrosion behavior of carbon steel in soil. *Int. J. Corros.* **2018**, 1–14 (2018).
70. Li, E. et al. Electron donor dependent inhibition mechanisms of D-phenylalanine on corrosion of Q235 carbon steel caused by Desulfovibrio sp. Huiquan2017. *Corros. Sci.* **188**, 109493 (2021).
71. Wu, J. et al. The influence of Desulfovibrio sp. and Pseudoalteromonas sp. on the corrosion of Q235 carbon steel in natural seawater. *Corros. Sci.* **112**, 552–562 (2016).
72. Li, Z., Wu, W., He, Y. & Du, C. W. Comparison of microbiologically influenced corrosion of structural steel by nitrate-reducing bacteria in aerobic and anaerobic conditions. *Constr. Build. Mater.* **288**, 123091 (2021).
73. Lu, X., Liu, Y., Liu, M. & Wang, Z. Corrosion behavior of copper T2 and brass H62 in simulated Nansha marine atmosphere. *J. Mater. Sci. Technol.* **35**, 1831–1839 (2019).
74. Pineau, S. et al. Formation of the Fe(II–III) hydroxysulphate green rust during marine corrosion of steel associated to molecular detection of dissimilatory sulphite-reductase. *Corros. Sci.* **50**, 1099–1111 (2008).
75. Xu, Y., Huang, Y., Cai, F., Lu, D. & Wang, X. Study on corrosion behavior and mechanism of AISI 4135 steel in marine environments based on field exposure experiment. *Sci. Total Environ.* **830**, 154864 (2022).
76. Muyzer, G. & Stams, A. J. M. The ecology and biotechnology of sulphate-reducing bacteria. *Nat. Rev. Microbiol.* **6**, 441–454 (2008).
77. Lovley, D. R. Extracellular electron transfer: Wires, capacitors, iron lungs, and more. *Geobiology* **6**, 225–231 (2008).
78. Lovley, D. R. Organic matter mineralization with the reduction of ferric iron: A review. *Geomicrobiol. J.* **5**, 375–399 (1987).
79. Michel, C., Brugna, M., Aubert, C., Bernadac, A. & Bruschi, M. Enzymatic reduction of chromate: Comparative studies using sulfate-reducing bacteria. *Appl. Microbiol. Biotechnol.* **55**, 95–100 (2001).
80. Takeuchi, M. et al. Methyloceanibacter caenitepidi gen. nov., sp. nov., a facultatively methylotrophic bacterium isolated from marine sediments near a hydrothermal vent. *Int. J. Syst. Evolut. Microbiol.* **64**, 462–468 (2014).

ACKNOWLEDGEMENTS

This work was supported by the Hainan Provincial Joint Project of Sanya Yazhou Bay Science and Technology City (No. 2021CXLH0005), the Key Research Program of Frontier Sciences, CAS (No. ZDBS-LY-DQC025), the Young Elite Scientists Sponsorship Program by CAST (No. YESS20210201), Wenhai Program of the S&T Fund of Shandong Province for Pilot National Laboratory for Marine Science and Technology (Qingdao) (No. 2021WHZZB2303), the National Natural Science Foundation of China (Nos. 42076044, 41706080 and 41806090), and Hainan Province Science and Technology Special Fund (No. ZDYF2021GXJS210).

AUTHOR CONTRIBUTIONS

X.D.: Methodology, software, investigation, writing—original draft; Y.Z., J.Y., F.G., R.Z., and J.S.: Resources, visualization, investigation; X.Z. and J.D.: Writing—review & editing, conceptualization, supervision, project administration, funding acquisition; B.H.: Supervision.

COMPETING INTERESTS

The authors declare no competing interests.

ADDITIONAL INFORMATION

Supplementary information The online version contains supplementary material available at https://doi.org/10.1038/s41529-022-00304-7.

Correspondence and requests for materials should be addressed to Xiaofan Zhai or Jizhou Duan.